Journal of Materials Chemistry A

PAPER

View Article Online
View Journal | View Issue

Cite this: J. Mater. Chem. A, 2015, 3, 18675

Fish scale inspired design of underwater superoleophobic microcone arrays by sucrose solution assisted femtosecond laser irradiation for multifunctional liquid manipulation†

Guoqiang Li,[a] Yang Lu,[b] Peichao Wu,[a] Zhen Zhang,[a] Jiawen Li,*[a] Wulin Zhu,[a] Yanlei Hu,[a] Dong Wu*[a] and Jiaru Chu[a]

Received 13th July 2015
Accepted 4th August 2015

DOI: 10.1039/c5ta05265c

www.rsc.org/MaterialsA

The preparation of superhydrophilic/superoleophilic/underwater superoleophobic surfaces is inspired by natural surfaces such as fish scales possessing hierarchical micro/nanostructures. In this paper, we report the assembly of self-organized hierarchical microcone arrays on a nickel surface by sucrose solution-assisted femtosecond laser irradiation. The processed surface is superhydrophilic (13.47°–4.01°), superoleophilic (7.45°–3.73°), and underwater superoleophobic (135.22°–166.16°) which are comparable to those of fish scales. The wettabilities of the processed surfaces are tunable by adjusting the mass ratio of sucrose to water and pulse energy to control the height (1.62–10.34 μm) and size (2.1–2.81 μm) of the microcones. Multifunctional liquid manipulation such as microdroplet transferring, static and dynamic storage, liquid transportation and mixing is demonstrated. Our proposed method features rapidness, simplicity and ease of large-area fabrication, which may find broader applications in many fields such as microfluidic devices, fluid microreactors, biomedicine, biomedical scaffolds, and chemical–biological sensors.

1. Introduction

After billions of years of evolution, fishes have developed perfect underwater superoleophobic ability, which makes their bodies well protected from oil contamination in aqueous environments, exhibiting appealing properties such as self-cleaning and anti-fouling.[1–3] It is reported that fish scales consist of superhydrophilic micropapillae covered with nanostructures, exhibiting superhydrophilicity in air.[1,4] Hence, water can be trapped in the hierarchical micro/nanostructure to form an oil-repellent layer, leading to underwater superoleophobicity and ultralow oil-adhesion.[1,4] Inspired by fish scales, many kinds of underwater superoleophobic and low-adhesive interfaces have been fabricated with diverse technologies to boost their applications in self-cleaning coatings, fluidic devices, oil/water separation, bioadhesion, oil-droplet manipulation and so on. For example, conventional top-down microfabrication methods,[5–8] consisting of etching,[6] lithography,[7] and anodization,[8] have been widely used in underwater superoleophobic surface fabrication due to their simplicity and cheapness. However, these methods have many drawbacks such as the fabricated surfaces being fragile, or processes needing a long molding cycle, and even formation of residual solutions which will pollute the environment. On the other hand, bottom-up methods[5,9–15] including electro/spray/vapor/deposition,[9,10] hydrothermal methods,[11] sol–gel processes,[12] dip coating,[13] self-assembly,[14] and template methods[15] are also used for fabricating underwater superoleophobic surfaces due to their cheapness. Nevertheless, these methods need complex multi-step manipulation. Therefore, new routes to effectively and economically produce such functional surfaces with large area are still highly desirable.

Laser processing has emerged as an innovative method to prepare special surface micro/nanostructures overcoming the disadvantages of traditional methods.[4,5,16–18] It is a one-step and fast method without the need for a mask or a harsh environment.[5] In addition, the surface structures, even complex 3D structures can be controlled by modulating the processing parameters.[17] For example, Chen *et al.*[16,18] have put forward an effective method for preparing underwater superoleophobic surfaces by femtosecond laser microfabrication on Ti materials. As a kind of important ferromagnetic metal, nickel shows outstanding optical, catalytic, electrical, and superior resistant characteristics to corrosion, which makes it widely applicable in electronic devices,[19] nickel-batteries,[20] alloys,[21] and chemical catalysts.[22] However, studies on the present fabrication on nickel materials using femtosecond laser microfabrication and

[a]Micro/Nano Engineering Laboratory, University of Science and Technology of China, Hefei, Anhui, 230026, PR China. E-mail: jwl@ustc.edu.cn; dongwu@ustc.edu.cn

[b]Precision and Equipment Support Laboratory, Department of Instrument Science & Opto-Electronics Engineering, Hefei University of Technology, Hefei, Anhui, 230009, PR China

† Electronic supplementary information (ESI) available. See DOI: 10.1039/c5ta05265c

underwater superoleophobicity are still few. Therefore, it is of great interest to produce underwater superoleophobic surfaces on nickel substrates, and study their functions and potential applications.

Here, we demonstrate a facile and rapid method to fabricate large-area microcone arrays by one-step femtosecond laser irradiation on nickel targets in sucrose solutions. The prepared surfaces are superhydrophilic in air and superoleophobic in water. It is indicated that the height and size are tunable by controlling the ratio of sucrose to water in solution and the laser pulse energy, leading to controllable wettabilities for water and oil. Furthermore, these processed surfaces covered with microcone arrays exhibit multiple functions, which can be used in microfluidic devices, fluid microreactors, biomedicine, biomedical scaffolds, and chemical and biological sensors.

2. Experimental section

2.1. Materials

Nickel sheets with a purity of 99.99% were purchased from New Metal Material Tech. Co., Ltd, Beijing, China. The oil used in our experiment is 1,2-dichloroethane, and its chemical formula is $C_2H_4Cl_2$. Sucrose (chemical formula is $C_{12}H_{22}O_{11}$ and the relative molecular mass is 342.3), milk (the color is white) and red ink are purchased from a supermarket. The sucrose solution is prepared by dissolving a certain mass of sucrose in 100 g distilled water, and the mass ratio ranges from 10 : 100 to 70 : 100.

2.2. Structuring nickel surface

A regenerative amplified Ti:sapphire femtosecond laser system (Legend Elite-1K-HE, Coherent, America) that generates 104 fs pulses at a repetition rate of 1 kHz with a central wavelength of 800 nm is employed for irradiation. The focused spot at the nickel surface through the sucrose solution layer is about 30 μm. To structure the nickel surface, the incident laser pulse energies are set from 0.10 to 0.20 mJ per pulse, the scanning speed is 1 mm s^{-1}, and the step size between the adjacent scanning lines is 50 μm.

2.3. Characterization of the structured nickel surface

After laser processing, the structural properties of the samples are observed by using a scanning electron microscope (SEM, JSM-6700F, JEOL, Tokyo, Japan). The surface structures are studied by X-ray diffraction spectra measurements. The contact angles of 5 μl water or oil droplet and the sliding angles of the oil droplet underwater are measured by using a contact-angle system (CA100D, Innuo, China). The average values are obtained by measuring five drops at different locations on the same surface.

3. Results and discussion

3.1. One-step formation of superhydrophilic and underwater superoleophobic microcone arrays

Fig. 1(a) shows that the nickel surface irradiated in the sucrose solution with a mass ratio of 55 : 100 for sucrose and water and a laser pulse of 0.19 mJ displays a gray color. It is found that the water rapidly spreads out once it contacts with the structured surface. The measured contact angle is less than 5°, exhibiting superhydrophilicity.[1,4] Furthermore, the oil droplet can spread out much faster than water and forms a smaller contact angle due to the smaller surface tension of oil than that of water, displaying superoleophilicity in air.[1,4] In contrast, the processed nickel surface shows underwater superoleophobicity with an oil contact angle of nearly 170°.[1,4]

Previously, we have reported the assembly of self-organized 3-dimensional porous nickel micro/nanocage arrays by ethanol-assisted femtosecond laser irradiation.[17] In direct contrast to the irradiation in sucrose solution, the processed nickel surfaces show a black color, and the surface is hydrophobic and oleophilic in air [Fig. 1(d)]. The formation of the hydrophobic and oleophilic surface is related to the laser induced surface rough porous micro/nanocage structures [Fig. 1(e)] and the chemical composition. The XRD analysis verified NiO was formed after the ethanol-assisted femtosecond laser irradiation [Fig. 1(f)],[23] and the chemical formula can be described as

$$Ni + C_2H_5OH \rightarrow NiO \quad (1)$$

The micro/nanostructures formed in the two liquids are very different [Fig. S1, ESI†]. In sucrose solution, hierarchical cone arrays with a size (here, we define the size of the cone as the cone bottom radius, which is labeled as "*R*" in figures) of 3 μm covered by 10–30 nm nanovillus structures are induced [Fig. 1(b)]. In addition, it is almost difficult to see the flame and there appear only a few bubbles during the course of irradiation. The processing in sucrose solution is peaceful. These distinct features promote the formation of hierarchical cone arrays. The nickel with a clean surface is initially hydrophilic. In addition, the XRD study shows that there is no chemical change on the irradiated nickel,[23] so the produced pure nickel roughness enhances the hydrophilicity in air [Fig. S2, ESI†].

3.2. Precisely controlling the growth of the cone by adjusting the mass ratio of the sucrose solution and the laser pulse energy

From the aspect of practical application, it is acceptable to fabricate the controllable structures *via* a simple parameter. According to the experimental observation, it is found that two critical parameters, namely the mass ratio of sucrose to water in the solution and laser pulse energy should be carefully controlled. In experiments, four typical mass ratios ranging from 10 : 100 to 55 : 100 with pulse energies ranging from 0.10 to 0.19 mJ were examined [Fig. S3 and S4, ESI†]. It is easily seen that the mass ratio of the solutions greatly affected the cone topography. With the increasing mass ratio, the refractive index and viscosity of the solution can be sharply increased, leading to the stronger penetration into the nickel sheet, which plays an obvious role in the growth of the height and size. For example, when the mass ratio is increased from 10 : 100 to 55 : 100, the height and the size can increase from 1.62 to 8.02 μm and 2.1 to 2.63 μm at a pulse energy of 0.10 mJ, respectively. In addition, the laser pulse energy was also used to control

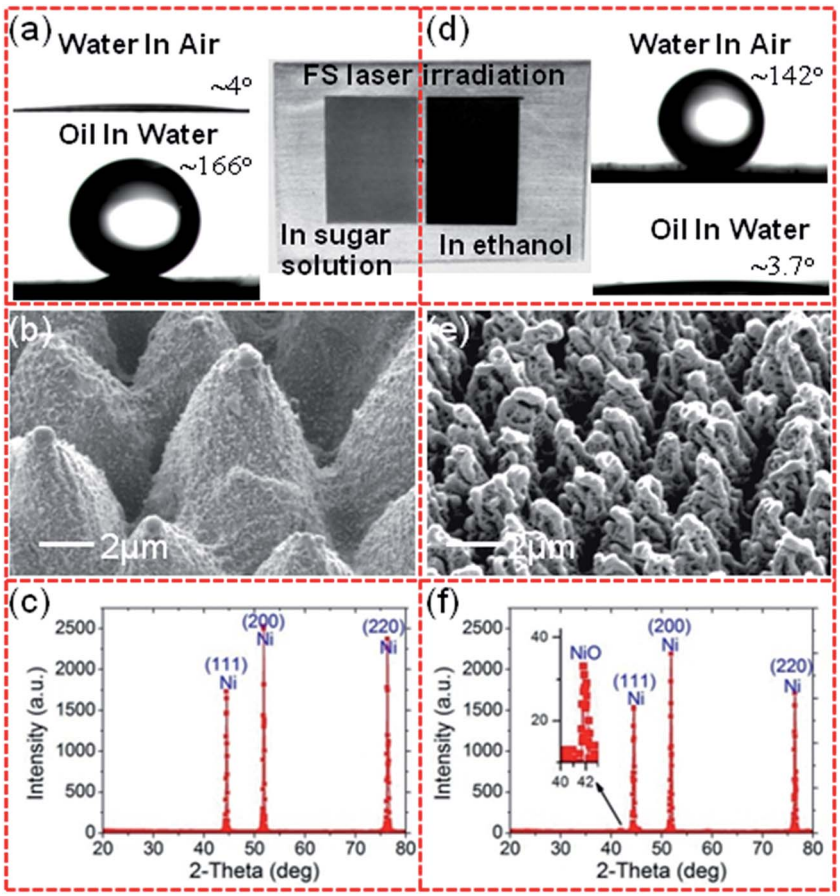

Fig. 1 The preparation of microcones by sucrose solution-assisted femtosecond laser irradiation. (a) The nickel prepared in sucrose solution displays gray color and the surface shows ultralow water CA 4° and underwater oil CA 166°. (b) The SEM images of the morphology of the surface structures prepared in sucrose solution. It is indicated that the structures formed in sucrose solution are hierarchical microcones with 3 μm size and 10.5 μm height. (c) The XRD analysis shows that no chemical changes happen in sucrose solution. (d) The surface processed in ethanol exhibits black color, and it is hydrophobic with water CA 142° and underwater oil CA 3.7°. (e) SEM results indicate that the structures formed in ethanol are porous micro/nanocages with 1.6 μm size and 6.5 μm height. (f) The XRD results show that NiO is generated in ethanol.

cones. As the pulse energy increases, the cones become larger due to the stronger interaction of laser with nickel surfaces. Taking a mass ratio of 10 : 100 for example, at a low pulse energy of 0.10 mJ, the laser can only induce a small cone with a height of 2.14 μm and a size of 2.31 μm. With the increase of pulse energy, the laser-induced plasma is further expanded to produce a stronger shock wave, higher temperature and higher pressure at the interface, so higher and larger cones are produced.[17] By carefully modulating these two parameters, a series of representative microcone arrays are prepared [Fig. 2]. It is noteworthy that the growth rate of the cone height caused by the mass ratio is faster than that of the pulse energy. The possible reasons for the growth of the cones are the higher boiling point and higher viscosity of the sucrose solutions with greater mass ratio.

The laser induced cone arrays are schematically illustrated in Fig. 3(a), and the height and size for a single cone can be standardized as in Fig. 3(b). In order to further investigate the influence of the mass ratio and pulse energy on the growth of the cones, the heights and the sizes as a function of pulse energy under different mass ratios are indicated in the histogram statistics [Fig. 3(c) and (d)], respectively. The statistical results demonstrated that the height and the size can be effectively modulated in the ranges of 2.1–2.81 μm and 1.6–10.34 μm, respectively. Compared with other methods reported before, our proposed method featured simplicity and flexibility.

3.3. The wettabilities of the microcone arrays

The water contact angle of the flat nickel surface in our experiment is $\theta_{WA} = 58.26°$ [Fig. S5(a), ESI†], showing intrinsically weak hydrophilicity in air. As mentioned above, its wetting property can be tuned to be more hydrophilic and even superhydrophilic by the laser-induced rough hierarchical micro/nanostructures.[1,3] The roughness factor of the structures in our case can be defined as the ratio of the actual apparent surface area to geometric projected area,[24] and the expression is shown as

$$r = \sqrt{1 + \left(\frac{H}{R}\right)^2} \quad (2)$$

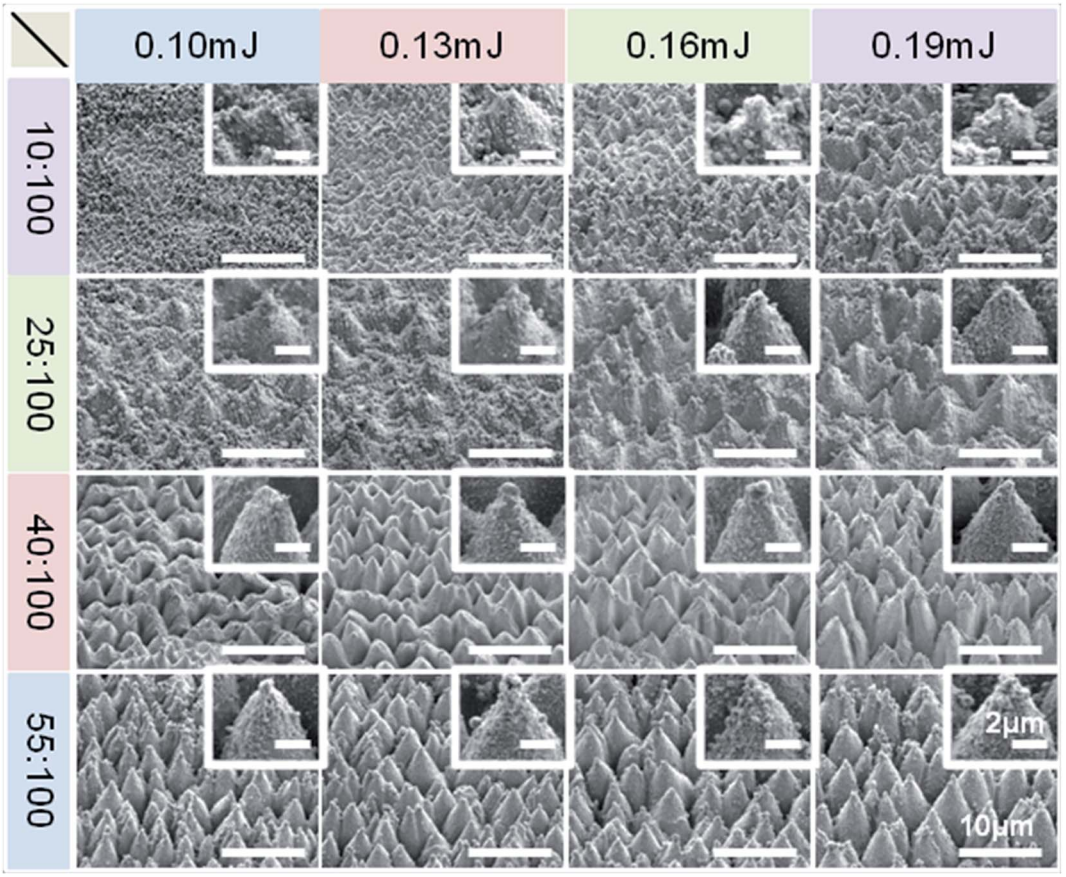

Fig. 2 45° tilted SEM images of the samples by femtosecond laser irradiation in sucrose solution with different mass ratios and laser pulse energies. The insets show the magnified SEM images for microcones, and the bar is 2 μm. These results indicate that the size and the height of the laser induced microcones can be tuned from 2.1 to 2.81 μm and from 1.62 to 10.34 μm, respectively, by adjusting the mass ratio of the sucrose solution and the laser pulse energy. In addition, all the microcones are distributed into periodical arrays. From the magnified SEM images, it is observed that the microcones are covered by microvilli. These hierarchical multi-level microstructures can further enhance their wetting properties.

The roughness factor based on the data in Fig. 3(c) and (d) is calculated [Fig. 4(a)].[17] It is indicated that the roughness factor increased with the increasing microcone height and size. In addition, the nanoscale structures on the microcone also increase the superficial area of micro/nanocages, which further enhances the roughness factor. By introducing the roughness, the water contact angle of the nickel surface is modified to less than 14° [Fig. 4(b)]. Due to the hydrophilicity, the water can completely contact the rough surface, as shown in the schematic diagram of Fig. 4(b). The contact model for this case is described by the Wenzel model[25,26] as follows

$$\cos \theta'_{WA} = r \cos \theta_{WA} \quad (3)$$

where θ'_{WA} and θ_{WA} are the water contact angle on the structured surface and flat surface, respectively. According to Wenzel's model, the hydrophilic surfaces will be more hydrophilic with the increase of roughness. In addition, it can be observed that most surfaces are modified to be superhydrophilic with a contact angle less than 10°, and the minimum value is as small as 4°. On the other hand, the contact angle for oil on flat nickel is $\theta_{OA} = 26.04°$ [Fig. S5(b), ESI†], but all the contact angles on rough ones are below 7.5° [Fig. 4(c)], much less than that of water, demonstrating superoleophilicity. This is because of the lower surface tension of oil than that of water, which enables the oil droplet to be more easily spread on the rough nickel surface. Similarly, the oil contact angle is decreased with the increasing roughness, and the minimum value reached 3.5°.

It is indicated that the hydrophilic flat nickel surface is tuned to be an oleophobic one when it is immersed in water. Deduced from Young's equation,[1,27] the oil contact angle can be described as the following equation:[1,27–30]

$$\cos \theta_{OW} = \frac{\gamma_{OA} \cos \theta_{OA} - \gamma_{WA} \cos \theta_{WA}}{\gamma_{OW}} \quad (4)$$

where θ_{OW} is the contact angle of oil on a flat surface in water. γ_{OW}, γ_{OA}, and γ_{WA} are the surface tensions of the oil/water, oil/air, and water/air interfaces. For 1,2-dichloroethane, the surface tension with air and water are 24.15 and 28.1 mN m^{-1}, respectively.[1] The water surface tension is 73 mN m^{-1} at room temperature. Calculated from eqn (4), the oil contact angle on the flat nickel surface in water is 126.47°, which is in good agreement with the measured value of 124.13° [Fig. S5(c), ESI†].

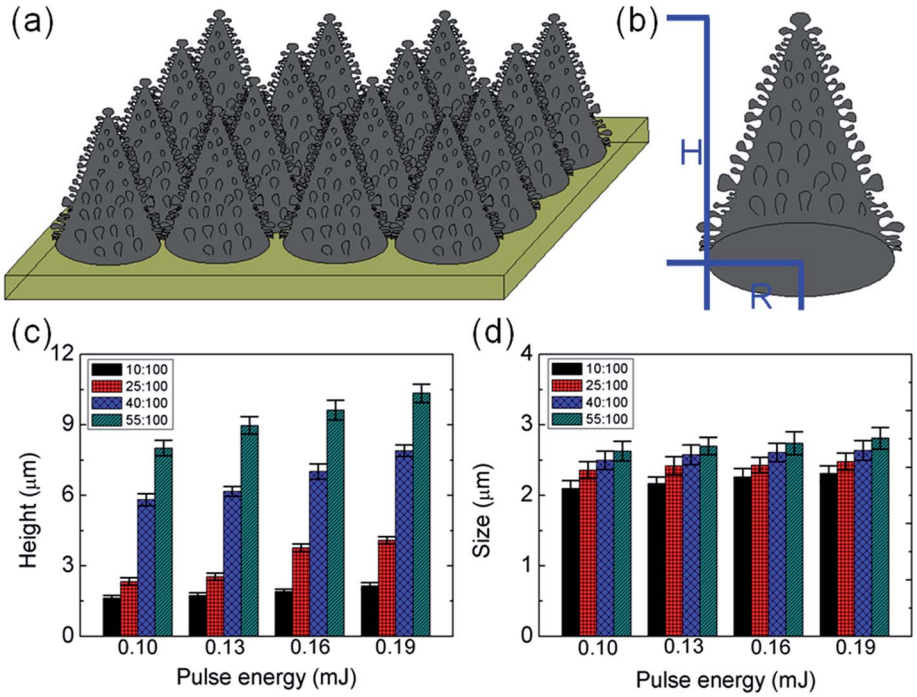

Fig. 3 (a) Schematic diagram for the prepared microcone arrays. The microcone consists of the standard cone and the ambient villus nanostructures, which endows the microcones with hierarchical structures. (b) The schematic diagram of a single magnified microcone. The height (*H*) and the size (*R*) of the microcone are marked in the figure. (c and d) The statistical height and size of the microcones, which are obtained by calculating the average value. At each given mass ratio of the sucrose solution, the height and the size become bigger with the increasing pulse energy, but the growth rates are lower. In addition, at a given pulse energy, the growth rate of the height is larger than that of the size.

In Fig. 4(d), it is found that the underwater oleophobic flat nickel surface is tuned to be more oleophobic ($135.22^\circ < \theta_{OW} < 150^\circ$) and even superoleophobic ($\theta_{OW} > 150^\circ$) by introducing the microcones. When the nickel is immersed in water, the processed area can be entirely wetted by water due to the superhydrophilicity.[1] The water molecules can be trapped in the micro/nanostructures when the oil drop comes into contact with the processed surface, developing a composite water/solid interface. For the incompatibility, the trapped water acts as an insulation layer to prevent the oil droplet from permeating into the micro/nanostructures. In this case, the oil droplet can only contact the top of the induced micro/nanostructures, displaying oleophobic or superoleophobic surfaces in water.[1] The state of the oil droplet can be described by the Cassie model,[1,27,31,32] and the contact angle can be expressed as

$$\cos \theta'_{OW} = f \cos \theta_{OW} + f - 1 \quad (5)$$

where θ'_{OW} is the contact angle of oil on the rough surface in water. f is the area fraction of the solid, which is defined as the ratio of the actual contact area by the oil droplet to the whole area of the cone. Although the exact value of f is not readily available, it can be theoretically deduced from eqn (5), as shown in Fig. 4(e). In our study, the area fraction f is below 0.66, and the value decreases when the roughness increases. According to eqn (5), for a rough nickel surface, the contact angle for underwater oil droplet is increased with decreasing area fraction.

It is observed from Fig. 4(d) that the measured contact angles on some surfaces with smaller roughness are below 150°. According to the reported studies, these structured surfaces are in metastable Wenzel/Cassie hybrid states[33,34] as shown in the schematic diagram of Fig. 4(f_1). It is stated that some part of the oil droplet can homogeneously wet the rough surface, while the other part shows heterogeneous wetting, which can be more clearly observed from the magnified illustration in Fig. 4(f_2). When the contact angle is above 150°, the contact is the Cassie model. In this case, the state represents a non-wet-contact mode, where the oil contacts the upper end of the microcones, leaving the lower end immersed in water, as shown in Fig. 4(f_3). Especially, as indicated in Fig. 4(f_4), when the area fraction f is about 0.066, the contact angle can nearly reach 170°, in which the oil droplet only contacts the peak of the cones, demonstrating extreme underwater superoleophobicity.

Based on the above discussion, our prepared microcone arrays have the key properties of superhydrophilicity, superoleophilicity and underwater superoleophobicity, which are very similar to the features of the fish scales. Furthermore, it is indicated that all these wettabilities can be easily tuned over a wide range by adjusting the mass ratio and pulse energy.

3.4. The liquid manipulation

3.4.1. Liquid droplet transferring. It is reported that the oil can easily roll off the fish scales, keeping the fish body clean in contaminated water. The structured nickel surfaces have

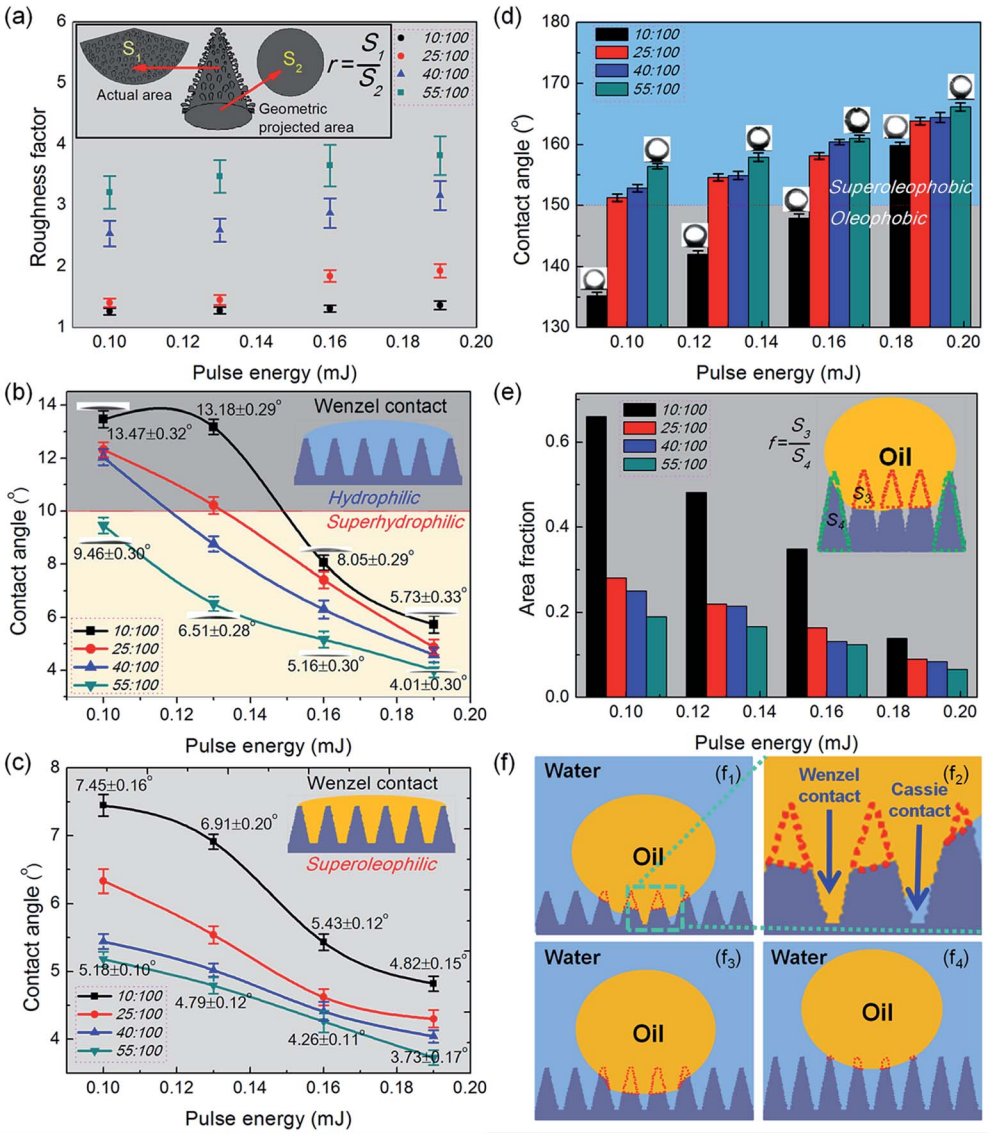

Fig. 4 The wettabilities of the laser induced microcone arrays. (a) The calculated roughness factor for the microcone arrays. The insets are the model of the microcone and the calculation formula. The roughness factor is defined as the ratio of the actual apparent surface area (S_1, the sector) to the geometric area (S_2, the circular). The roughness factors increased with the increasing mass ratio and pulse energy. (b and c) The water and oil contact angles. The processed surfaces are superhydrophilic and superoleophilic and the contact models are the Wenzel state. All contact angles decreased with the increasing roughness factor. (d) The surfaces are underwater superoleophobic and the oil contact angles increased with the increasing roughness factor. (e) The calculated area fraction which is defined as the ratio of actual contact area (S_3) by the oil droplet to the whole area of the cone (S_4). It is demonstrated that the area fractions decreased with the increasing roughness factor. (f) The detailed contact model for underwater oil. When the contact angle is smaller, the contact model is metastable Wenzel/Cassie hybrid states. However, if the contact angle is larger, the contact model is the Cassie state.

similar self-cleaning effects to fishes, which can be verified by measuring the oil sliding angle (SA) [Fig. 5(a)].[35,36] We found that the surfaces with different roughnesses showed different oil adhesions and SAs. The adhesion difference is ascribed to the distinct contact models. In the metastable state [Fig. 4f_1 and f_2],[33,34] the oil droplet partially wets the microcones and the oil sliding angle is higher than 9°. According to our previous discussion, the metastable states should appear in the region where the $CA_{OW} \leq 150°$, marked above the dashed line in Fig. 5(a). In contrast, below the dashed line, the contact modes belong to Cassie's state.[1,27] The oil droplet can slide on the surface at a smaller sliding angle with lower adhesion. Especially, at a CA_{OW} nearly 170°, there is hardly any contact space between the oil droplet and the rough structures, so that the adhesion is extremely low and the oil droplet easily rolls off with the surface slightly tilted at only 2°. This study indicates the adhesion force can be controllably tuned from the metastable state with high adhesion to the Cassie state with ultralow adhesion.

The sliding behaviors of three structured surfaces named "A", "B", and "C" are studied in detail [Fig. 5(b)]. Fig. 5(b) shows the time sequences of snapshots of a 5 μl oil droplet rolling on

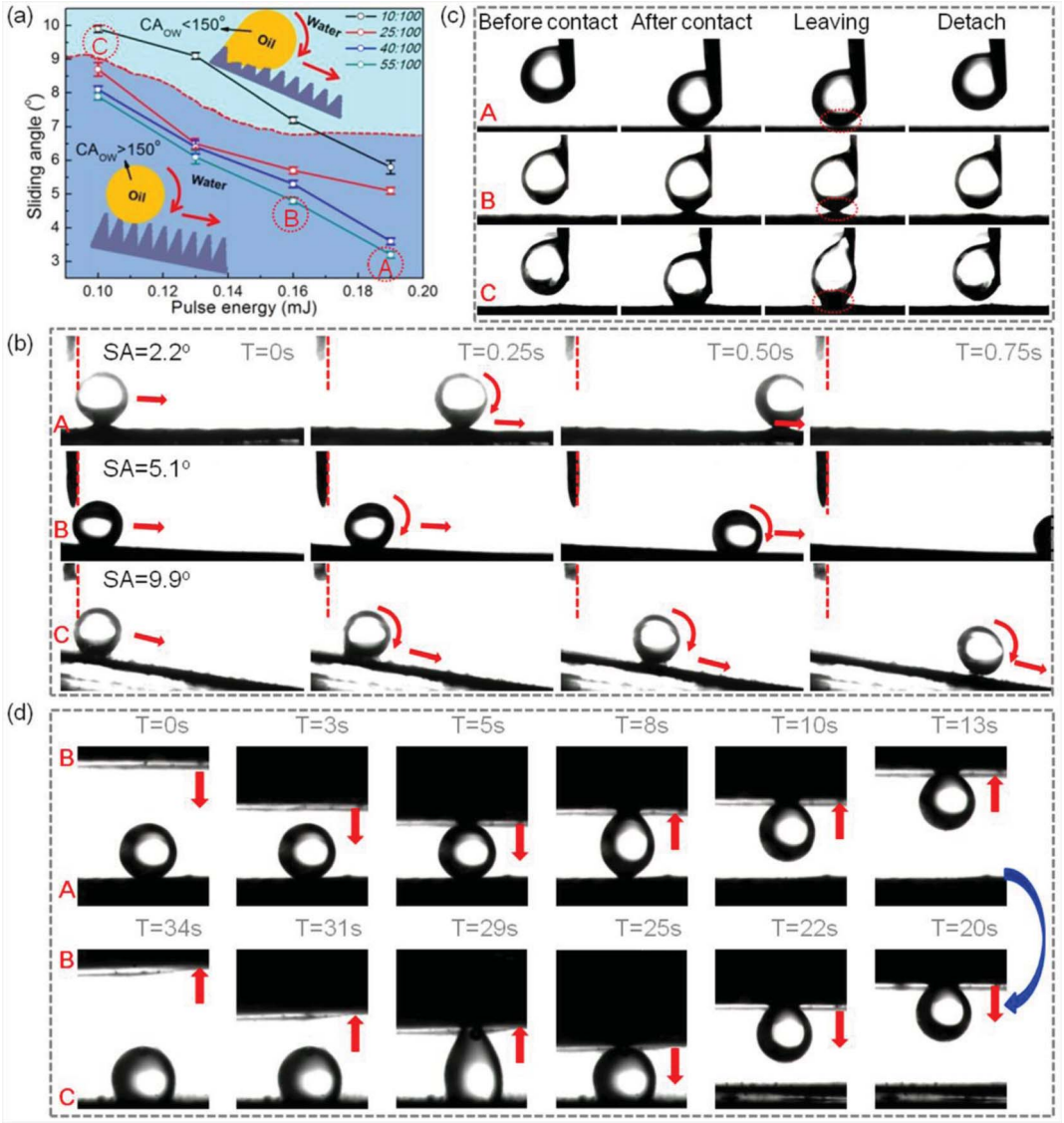

Fig. 5 The adhesion contrast and the underwater oil transferring experiment. (a) The sliding angle of the underwater oil. It is indicated that the SAs decreased with the increasing mass ratio and pulse energy. (b) The time sequences of snapshots of oil rolling on the three kinds of structured surfaces. It can be seen that the oil droplet can roll easily even when the A surface is slightly tilted. The oil droplet only moves a shorter distance on the B surface than that on A at the same time. While for the C surface, the oil droplet slides with an extremely slow speed even when the surface is tilted about 9.9°. (c) Dynamical adhesive force behaviors on A, B and C surfaces. During the leaving process, it is found that the contact areas are different, presenting distinct adhesive behaviors. (d) Process of transferring the oil droplet from the A surface to the C surface *via* the B surface. Utilizing the differences of the adhesive force, the structured surfaces can be used as the "mechanical hand" to transfer the oil droplet from the lower adhesive surface to the higher one.

the three surfaces. It can be seen that the oil droplet can move easily when the A surface is only slightly tilted 2.2°, and it rolls off the entire surface in a very short time [supporting video 1, ESI†]. On the contrary, the oil can only slide a short distance on the B surface in the same time, and possesses a SA of 5.1° [supporting video 2, ESI†]. As for the C surface, the oil droplet slides with an extremely slow speed even when the surface is tilted about 9.9° [supporting video 3, ESI†].

Another experiment about their adhesive behavior is conducted by controlling the oil droplet to contact and leave the A, B, and C surface [Fig. 5(c)].[36–38] For the A surface, during the whole course of contact and leave, the shape of the oil droplet remains spherical, with almost no changes, showing a very small adhesive force. In this case, the oil droplet can be transferred away without any loss. For the B surface, it is found that the oil droplet is first elongated to elliptical, and has a certain contact area with the B surface when it is about to leave. This phenomenon indicates that the B surface has larger adhesive force than that of the A surface. It is observed that the oil droplet is seriously deformed into a long elliptical shape and has a large contact area when it is pulled from the C surface, revealing strong adhesion.

These surfaces could be applied in the manipulation of oil droplets by transferring them from a lower adhesive surface to a

higher one, which have key potential applications in biomedical fields.[36,38–40] Fig. 5(d) shows an example of transferring a 5 μl oil droplet. First, the oil droplet is placed at the low adhesive A surface. Then, the medium adhesive B surface is used as a "mechanical hand" to capture the oil droplet and release it onto the C surface.

3.4.2. Liquid storage. Due to the superhydrophilcity and superoleophilicity, the as-prepared nickel surfaces can be used for liquid storage.[41,42]

Static storage. As shown in Fig. 6(a), milk, red ink, and oil are dripped onto the processed ring-shaped area with 5 mm diameter, forming 3 × 3 arrays. It is found that none of the droplets overflow from the designated circular regions, displaying ultrahigh adhesion. In addition, the droplets still firmly adhere to the surface even if it is tilted at a certain angle for more than an hour. With this method, a few microliters to several milliliters and an even larger dosage of various liquids can be stored at the designated area [Fig. S6, ESI†].

Dynamic storage. In addition to the static storage, the surface can also serve as a stable storage media for storing the flowing fluid. As shown in Fig. 6(b), a 5 ml water droplet can be first fixed at the central circle. Then the water will flow in all directions under wobbling. Finally, the water can be captured by the surrounding arrayed circles. In this way, the flowing liquid can be stored successfully. This novel liquid storage technology may find applications in fixing reagent in gas liquid reaction in sensing system, collecting water and fog in hydropenic environment.

3.4.3. Liquid transportation. Fig. 6(c) shows the transportation dynamics of 5 ml red ink droplet pipetted on the processed surface [supporting video 4, ESI†]. The track of the red ink is marked with a red dotted line in each figure. It is found that the red ink immediately flows along the set path once it contacts the starting point, and rapidly travels over 50 mm in less than 6 s. It is thought that the extremely strong driving force is derived from the wicking force due to the surface superhydrophilicity. This experiment indicates that a regular nickel surface can be readily transformed to a superwicking one, which may find potential applications in microfluidics, lab-on-chip, and so on.[43,44]

3.4.4. Liquid mixing. Previous discussion indicates that in water, the untreated nickel is oleophobic, while the treated one is superoleophobic. By taking advantage of this property, we have designed a path to form a hollow "Y" shape, as shown in Fig. 6(d), composed of an untreated fine line and treated thick lines on both sides. In this way, the fine line can grasp the oil droplet and control it to move along the setting path, and the ultralow adhesion force of the processed lines on both sides

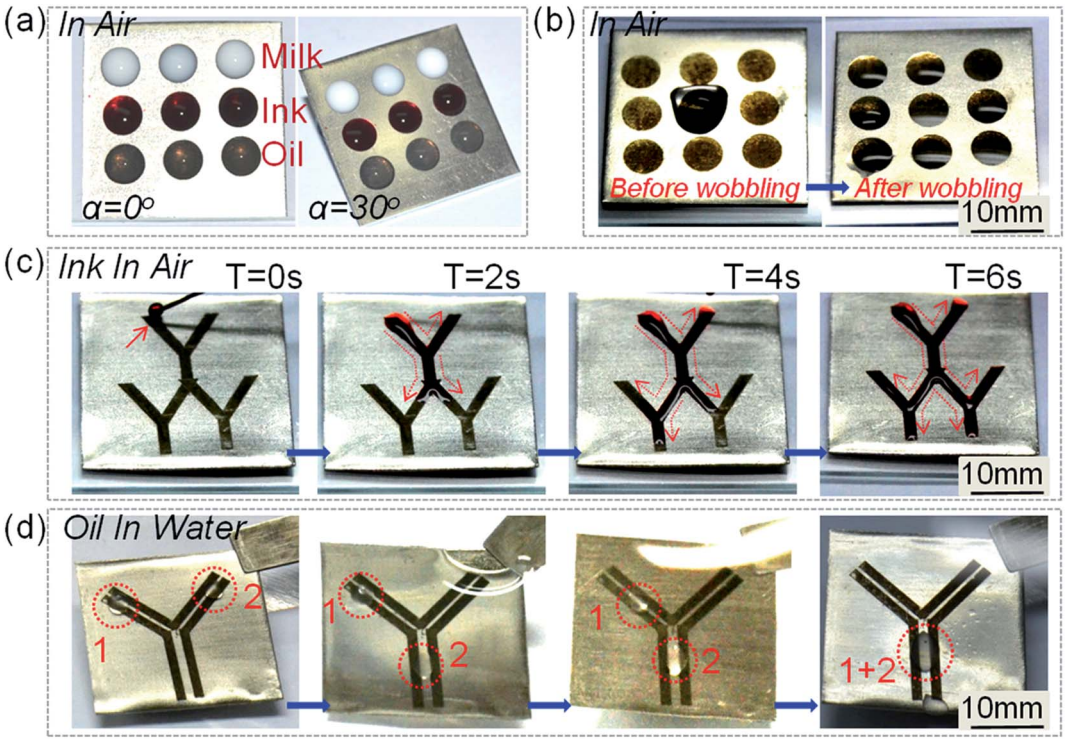

Fig. 6 The liquid manipulation experiments. (a) The static storage for milk, ink and oil. Due to the superhydrophilcity in air, the liquid can be firmly fixed at the processed areas on the horizontal and oblique surface. (b) The dynamic storage for water. The 5 ml water droplet can be fixed at the central circle, and then it will flow in all directions under wobbling the sample. Due to the superhydrophilcity, water can be captured and stored by the surrounding arrayed circles. (c) The capillary force driving property for red ink. The red ink immediately flows along the set path once it contacts the starting point of the path, and rapidly travels longer than 50 mm in less than 6 s. (d) The mixing function for oil in water. The "Y" shaped lines consist of an untreated fine line and treated thick lines on both sides. By gently vibrating the sample, oil droplets "1" and "2" can travel along the "Y" shaped lines and finally mix at the bottom of the pattern without any loss.

ensures that the oil droplet moves without loss. As shown in Fig. 6(d), by gently vibrating the sheet, oil droplets "1" and "2" can travel along the "Y" shaped line and finally mix together.

4. Conclusion

In summary, inspired by the fish scales, hierarchical microcone arrays are one-step assembled on a nickel surface by sucrose solution-assisted femtosecond laser irradiation. The structured nickel surface is superhydrophilic, superoleophilic, and superoleophobic underwater, possessing similar properties to fish scales. In addition, by tuning the solvent environment and the pulse energy, the height and the size of the microcones can be controlled effectively. The controllable microcones endow the processed nickel surface with multifunctions, such as liquid transferring, storage, transportation and mixing. The unique wetting properties of the structured nickel open new applications in the fields of microfluidic devices, fluid microreactors, biomedicine, biomedical scaffolds, and chemical and biological sensors.

Acknowledgements

This work is supported by the National Natural Science Foundation of China (No. 51275502, 61475149, 51405464, 91223203, and 11204250), the Anhui Provincial Natural Science Foundation (No. 1408085ME104), and the National Basic Research Program of China (No. 2011CB302100).

References

1 M. Liu, S. Wang, Z. Wei, Y. Song and L. Jiang, *Adv. Mater.*, 2009, **21**, 665.
2 Y. Cai, L. Lin, Z. Xue, M. Liu, S. Wang and L. Jiang, *Adv. Funct. Mater.*, 2014, **24**, 809.
3 P. R. Waghmare, N. S. K. Gunda and S. K. Mitra, *Sci. Rep.*, 2014, **4**, 7454.
4 J. Yong, F. Chen, Q. Yang, G. Du, C. Shan, H. Bian, U. Farooq and X. Hou, *J. Mater. Chem. A*, 2015, **3**, 9379.
5 T. Jiang, Z. Guo and W. Liu, *J. Mater. Chem. A*, 2015, **3**, 1811.
6 S. Ji, P. A. Ramadhianti, T. B. Nguyen, W. D. Kim and H. Lim, *Microelectron. Eng.*, 2013, **111**, 404.
7 M. Im, H. Im, J. H. Lee, J. B. Yoon and Y. K. Choi, *Soft Matter*, 2010, **6**, 1401.
8 S. Anandan, T. N. Rao, M. Sathish, D. Rangappa, I. Honma and M. Miyauchi, *ACS Appl. Mater. Interfaces*, 2012, **5**, 207.
9 T. Darmanin and F. Guittard, *Soft Matter*, 2013, **9**, 5982.
10 M. A. Gondal, M. S. Sadullah, M. A. Dastageer, G. H. McKinley, D. Panchanathan and K. K. Varanasi, *ACS Appl. Mater. Interfaces*, 2014, **6**, 13422.
11 H. Wang and Z. Guo, *Appl. Phys. Lett.*, 2014, **104**, 183703.
12 G. Hayase, K. Kanamori, G. Hasegawa, A. Maeno, H. Kaji and K. Nakanishi, *Angew. Chem.*, 2013, **125**, 10988.
13 O. U. Nimittrakoolchai and S. Supothina, *J. Nanosci. Nanotechnol.*, 2012, **12**, 4962.
14 S. Pechook, N. Kornblum and B. Pokroy, *Adv. Funct. Mater.*, 2013, **23**, 4572.
15 X. Deng, L. Mammen, H. J. Butt and D. Vollmer, *Science*, 2012, **335**, 67.
16 J. Yong, F. Chen, Q. Yang, U. Farooq and X. Hou, *J. Mater. Chem. A*, 2015, **3**, 10703.
17 G. Li, J. Li, C. Zhang, Y. Hu, X. Li, J. Chu, W. Huang and D. Wu, *ACS Appl. Mater. Interfaces*, 2014, **7**, 383.
18 J. Yong, Q. Yang, F. Chen, H. Bian, G. Du, U. Farooq and X. Hou, *Adv. Mater. Interfaces*, 2015, **2**, 1400388.
19 G. C. Anyfantis, G. C. Papavassiliou, N. Assimomytis, A. Terzis, V. Psycharis, C. P. Raptopoulou, P. Kyritsisc, V. Thoma and I. B. Koutselas, *Solid State Sci.*, 2008, **10**, 1729.
20 S. J. Lenhart, D. D. Macdonald and B. G. Pound, *J. Electrochem. Soc.*, 1988, **135**, 1063.
21 S. Roy, T. Majhi, A. Kundu, C. K. Sarkar and H. Saha, *Sens. Lett.*, 2011, **9**, 1382.
22 A. G. Sergeev and J. F. Hartwig, *Science*, 2011, **332**, 439.
23 M. Chigane and M. Ishikawa, *J. Chem. Soc.*, 1998, **94**, 3665.
24 H. Nakae, R. Inui, Y. Hirata and H. Saito, *Acta Mater.*, 1998, **46**, 2313.
25 A. Lafuma and D. Quéré, *Nat. Mater.*, 2003, **2**, 457.
26 J. Liu, X. Feng, G. Wang and S. Yu, *J. Phys.: Condens. Matter*, 2007, **19**, 356002.
27 Z. Xue, Y. Cao, N. Liu, L. Feng and L. Jiang, *J. Mater. Chem. A*, 2014, **2**, 2445.
28 Q. Cheng, M. Li, Y. Zheng, B. Su, S. Wang and L. Jiang, *Soft Matter*, 2011, **7**, 5948.
29 B. A. Starkweather, X. G. Zhang and R. M. Counce, *Ind. Eng. Chem. Res.*, 2000, **39**, 362.
30 M. Jarn, B. Granqvist, J. Lindfors, T. Kallio and J. B. Rosenholm, *Adv. Colloid Interface Sci.*, 2006, **123**, 137.
31 J. Yong, Q. Yang, F. Chen, G. Du, C. Shan, U. Farooq, J. Wang and X. Hou, *RSC Adv.*, 2015, **5**, 40907.
32 J. Yong, Q. Yang, F. Chen, D. Zhang, H. Bian, Y. Ou, J. Si, G. Du and X. Hou, *Appl. Phys. A*, 2013, **111**, 243.
33 M. Nosonovsky, *Langmuir*, 2007, **23**, 9919.
34 C. Dorrer and J. Rühe, *Soft Matter*, 2009, **5**, 51.
35 B. Bhushan, K. Koch and Y. C. Jung, *Soft Matter*, 2008, **4**, 1799.
36 D. Wu, S. Wu, Q. Chen, Y. Zhang, J. Yao, X. Yao, L. Niu, J. Wang, L. Jiang and H. Sun, *Adv. Mater.*, 2011, **23**, 545.
37 D. Wu, S. Wu, Q. Chen, S. Zhao, H. Zhang, J. Jiao, J. A. Piersol, J. N. Wang, H. Sun and L. Jiang, *Lab Chip*, 2011, **11**, 3873.
38 J. Yong, F. Chen, Q. Yang, U. Farooq, H. Bian, G. Du and X. Hou, *Appl. Phys. A*, 2015, **119**, 837.
39 J. Yong, F. Chen, Q. Yang, D. Zhang, G. Du, J. Si, F. Yun and X. Hou, *J. Phys. Chem. C*, 2013, **117**, 24907.
40 J. Yong, Q. Yang, F. Chen, D. Zhang, U. Farooq, G. Du and X. Hou, *J. Mater. Chem. A*, 2014, **2**, 5499.
41 S. Yang, J. Ju, Y. Qiu, Y. He, X. Wang, S. Dou, K. Liu and L. Jiang, *Small*, 2014, **10**, 294.
42 J. Huang, Y. Lai, F. Pan, L. Yang, H. Wang, K. Zhang, H. Fuchs and L. Chi, *Small*, 2014, **10**, 4865.
43 A. Y. Vorobyev and C. L. Guo, *Appl. Phys. Lett.*, 2009, **94**, 224102.
44 A. Y. Vorobyev and C. L. Guo, *Opt. Express*, 2010, **18**, 6455.